Non-linear AUV Controller Design Using Logic-Based Switching PID Control

Tazden Sewell, Jared Padayachee *, and Glen C. Snedden

Discipline of Mechanical Engineering, University of KwaZulu-Natal, Durban, South Africa
Email: 216003489@stu.ukzn.ac.za (T.S.); padayacheej@ukzn.ac.za (J.P.), sneddeng@ukzn.ac.za (G.C.S.)
*Corresponding author

***Abstract*—The inspection of pipes without stopping pipeline operations is of industrial interest due to the inherent economic benefits. A pipe inspection robot design is proposed together with a suitable motion controller. The proposed robot is an Autonomous Underwater Vehicle (AUV) architecture that does not require shunting, draining or unearthing pipework for inspection purposes. This posed the challenge of controlling the AUV through a narrow pipe where manouvers are restricted. A set of general non-linear equations of motion were identified and refined using existing research and strip theory. The non-linear analytical model was implemented in Simulink to enable real-time monitoring and controller tuning. A non-linear controller based on a combination of classical PID theory and switching logic was developed to control the platform. The controller was transplanted into a Hardware-in-Loop (HIL) testing model developed with the Arduino and Simulink software suites. Pool tests measuring the parameters pitch and yaw angles showed that when operated independently with a 5° input, the maximum overshoot was 0.5° or 10% of the command value with a maximum angular velocity of 1.25°/s. When operated simultaneously, the overshoot rose to 30% with a constant error in the region of 1° over the target. Distance readings conducted with ultrasonic sensors to the pipe wall showed constant Sway-Heave bias errors from the centerline as −5 mm, and 4 mm, respectively, with an error range of 4 mm / −7 mm for Sway and 6 mm/ −4 mm for Heave. Pitch and heave motions were up to 18% faster than yaw and sway motions due to actuator orientation, with speeds of 6.25°/s and 40.57 mm/s, respectively. Despite the turbulence present during tests, the controller successfully drove the AUV to target positions through active flow and presented a reasonable basis for further refinement.**

***Keywords*—autonomous underwater vehicle, pipe inspection robot, Autonomous Underwater Vehicle (AUV) dynamics, Proportional-Integral-Derivative (PID) control system**

I. Introduction

Pipeline inspection is critical for maintaining water, oil and fuel transportation infrastructure. In 2017, a market intelligence study [1] found that as much as 37% of South Africa's water supply is lost through damaged and aged pipes. Water scarcity requires us to be more proactive in how we manage the resources that are available to us.

Pipe failure often leads to environmental disasters, as was the case in 2015 when 383,000 L of oil were released into the Pacific Ocean due to poor maintenance and inspection of the pipeline [2]. Pipe inspections detect issues before they become critical, therefore saving money, extending the lifespan of pipework, and avoiding major environmental disasters.

Pipe inspections are conducted in two ways: external inspection and internal inspection. External assessments often require excavating large pipe sections to allow for visual inspection and can be expensive and time-consuming [3]. Internal pipe inspection is of growing interest due to the wealth of information that can be obtained [4]. Internal pipe inspection tools can range from manual pipe endoscopes to larger industrial Pipe Inspection Gauges (PIG). An emerging field of pipe inspection lies in the form of robotic pipe crawlers. Mobile robotic pipe crawlers fulfil a gap in pipe inspection where it is not feasible or practical to commission a PIG in conditions such as very large concrete pipes, pipe systems with many bends or buried lines with no main pipe access ways. Pipe crawlers are categorized by their method of locomotion and are typically Wheeled [5], Screw [6], Inchworm, Walking [7] or Wall-driven types [8, 9]. These robots are often smaller, cheaper to produce, outfit and deploy in the field with limited resources.

There have been numerous attempts and patents at designing robotic pipe crawlers. A brief review of some of the designs includes work by Nayak *et al.* [10], who investigated a pipe crawling robot with flexible couplings to rotate the climbing head and simulate screw motion allowing it to scale near-vertical pipes. Hayashi *et al.* [11] looked at operating a pipe inspection robot in pipe flow using bladders to act as contact pads to resist the forces applied by the moving water. Wu *et al.* [12] looked at designing a miniature robot capable of swimming through flooded pipelines using ducted propellers rather than wheels or grippers and did not require expensive tether stations. However, the system was unsuitable for inspection missions due to its size. Nickols *et al.* [13]

Manuscript received August 25, 2023; revised October 13, 2023; accepted November 29, 2023; published March 22, 2024.

doi: 10.18178/ijmerr.13.2.227-240

investigated a similar case, using ultrasonic sensors on a radio-operated legged submarine to walk through a pipe.

Existing pipe crawling robots are limited by their ability to navigate pipes and may require draining of the line, which can be costly. An Autonomous Underwater Vehicle (AUV) based inspection robots that operates within a pipe represents a novel approach to pipe inspection that requires further research; however, they are constrained to pipes that operate at total or near-full capacity; otherwise, the robot would not function without additional locomotion features.

Developing a robot platform based on the function of an AUV allows for pipe crawling without the need for draining, shunting, or excavating the pipe. It is an attractive alternative to industry and may result in significant logistics and cost savings.

A pipe crawling AUV requires a controller that can keep the robot from crashing into the pipe wall and damaging equipment. This paper presents the research and development of a non-linear AUV model and controller based on classical PID theory and switching logic. The paper presents the analytical open loop and closed loop performance, a sonar algorithm to measure pipe wall distances, and the implementation of a tuned controller into an experiment conducted in a pool to measure its effectiveness compared to the theoretical model. The results show that the controller successfully drove the system to its target despite turbulence and other environmental disturbances in the tests.

II. AUV Development and Modelling

The AUV design was based on a modified DARPA SUBOFF submarine [14]. The designs were developed in SOLIDWORKS® 3D CAD and FDM 3D printed out of a combination of PLA and PETG materials, as shown in Fig. 1. The implementation followed a modular design philosophy, with critical functions such as pump actuators, ballast, and computational elements being implemented in different modular segments. The modular segments were concatenated to create the submarine profile. The CAD model was converted to .STEP format for use in Simulink. A simulation model was developed in conjunction with a physical prototype for testing purposes.

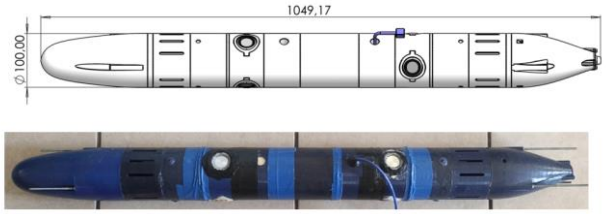

Fig. 1. AUV testing model.

A. General Equations of Motion

The general equations of motion served as the basis for developing a simulation model that characterized the response of the AUV to external forces while operating in water. The simulation model was used to obtain the open and closed loop responses necessary to develop and refine the controller design without requiring extensive physical testing.

The set of equations derived by Hagen and Gertler [15] described the dynamics of the AUV model for motion in six degrees of freedom. In practice, the six equations of motion are simplified based on the geometry of the AUV and the level of accuracy required for simulation. A critical aspect of this research was the identification of the appropriate hydrodynamic coefficients that allow the equations to accurately describe the dynamic response of the AUV when operating in a given fluid medium. The complete description of the motion relies on 36 coefficients, which are typically identifed through experimentation.

B. Applied Set of Equations

Literature and experimental data from the DARPA SUBOFF submarine project [16, 17] and similar literature on AUV design [18] was used to refine the dynamic model. The choice of a bare hull configuration reduced the required hydrodynamic coefficients from 36 to down to 7. The equations of motion account for the addition of seven jet thrusters located around the vessel, which control the axes of motion and were constructed by summing the forces acting on the AUV. The force components are arranged sequentially on the right side of the equations and are described in order as: hydrostatic (weight and buoyancy), added mass (forces due to pushing fluid out of the way), hydrodynamic (drag, moment and lift) and control forces (actuated jets, hydrofoils).

Surge (X) – Motion forwards/backwards

$$m(\dot{u} + qw - rv) = -(W - B)\sin\theta + \boldsymbol{X_{\dot{u}}}\dot{u} - \boldsymbol{Y_{\dot{v}}}(rv - qw) + \boldsymbol{X_{u|u|}}u|u| + \rho\frac{{Q_7}^2}{A_7} - \rho Q_7 u \quad (1)$$

Sway (Y) – Lateral motion sideways left/right

$$m(\dot{v} + ru - pw) = (W - B)\cos\theta\sin\phi + \boldsymbol{X_{\dot{u}}}ru + \boldsymbol{Y_{\dot{v}}}(\dot{v} - pw) + \boldsymbol{Y_{v|v|}}v|v| + \frac{\rho}{A_1\sqrt{2}}\left({Q_3}^2 + {Q_6}^2 - {Q_2}^2 - {Q_5}^2\right) \quad (2)$$

Heave (Z) – Vertical motion up/down

$$m(\dot{w} + pv - qu) = (W - B)\cos\theta\cos\phi - \boldsymbol{X_{\dot{u}}}qu + Y_{\dot{v}}(\dot{w} + pv) + \boldsymbol{Z_{w|w|}}w|w| + \frac{\rho}{A_1}\left({Q_1}^2 + {Q_4}^2\right) - \frac{\rho}{A_1\sqrt{2}}\left({Q_2}^2 + {Q_5}^2 + {Q_3}^2 + {Q_6}^2\right) \quad (3)$$

Pitch Moment (M) – Pitch about Y

$$\begin{aligned}\dot{q}I_y + pr(I_x - I_z) &= z_B B\sin\theta + x_B B\cos\theta\cos\phi \\ &+(\boldsymbol{X_{\dot{u}}} - \boldsymbol{Y_{\dot{v}}})uw + \boldsymbol{M_{q|q|}}q|q| \\ &+\frac{\rho L_J}{A_1}\left(\frac{{Q_2}^2 + {Q_3}^2 - {Q_5}^2 - {Q_6}^2}{\sqrt{2}} + {Q_4}^2 - {Q_1}^2\right)\end{aligned} \quad (4)$$

Yaw Moment (N) – Yaw about Z

$$\begin{aligned}\dot{r}I_z + pq(I_y - I_x) &= -x_B B\cos\theta\sin\phi - y_B B\sin\theta \\ &-(\boldsymbol{X_{\dot{u}}} - \boldsymbol{Y_{\dot{v}}})vu + \boldsymbol{N_{r|r|}}r|r| \\ &+\frac{\rho L_J}{A_1\sqrt{2}}({Q_3}^2 + {Q_5}^2 - {Q_2}^2 - {Q_6}^2)\end{aligned} \quad (5)$$

Roll Moment (K) – Roll about X

$$\begin{aligned}\dot{p}I_x + qr(I_z - I_y) &= -y_B B\cos\theta\cos\phi \\ &+z_B B\cos\theta\sin\phi\end{aligned} \quad (6)$$

C. Added Mass Coefficient Estimation

The added mass coefficients were required to fully describe the added mass inertial effects in the set of equations. The coefficients are typically obtained through rigorous experiments using scaled models with testing channels, however this was not practical for the scope of this paper, thus these coefficients were using the available data [16, 17] on the DARPA SUBOFF model and extrapolated for the modified test model used in this paper. Analytically, strip theory approximation [19, 20] was used as comparison for coefficients not obtained from existing research. The errors in estimating the coefficients were addressed through control system tuning. The following six equations are the analytical approximations of the hydrodynamic coefficients:

Added Mass in X axis due to surge

$$\boldsymbol{X_{\dot{u}}} \approx -0.1m \quad (7)$$

Added Mass in Y axis due to sway

$$\boldsymbol{Y_{\dot{v}}} \approx -\rho\overline{V_h} \quad (8)$$

Added Mass in X axis due to surge acceleration

$$\boldsymbol{X_{u|u|}} = -\frac{1}{2}(\rho A_f)c \quad (9)$$

Added Mass in Y/Z axis due to sway/heave acceleration

$$-\boldsymbol{Y_{v|v|}} = \boldsymbol{Z_{w|w|}} = -\frac{1}{2}(\rho A_f)b \quad (10)$$

Added Mass due to pitching about Y

$$\boldsymbol{M_{q|q|}} = -\frac{\rho}{12}\left(a\frac{w^2}{u^2} + b\frac{w}{u} + c\right)r_{hull}{l_{hull}}^4 \quad (11)$$

Added Mass due to yawing about Z

$$\boldsymbol{N_{r|r|}} = -\frac{\rho}{12}\left(a\frac{v^2}{u^2} + b\frac{v}{u} + c\right)r_{hull}{l_{hull}}^4 \quad (12)$$

The coefficients a, b, and c used in Eqs. (9)–(12) were obtained from the second-order polynomial approximation of Ridley [18]. The equations, shown in Eqs. (13)–(16), describe how the drag coefficient varies with changing angles of pitch and are well supported by experimental data. These coefficients were found by obtaining a set of drag values over a varying pitch range through CFD simulations and plotted against a 2nd order polynomial curve fit to obtain the empirical constants, these constants were independent of the speed of the test model and are presented as follows.

2nd order polynomial drag approximation due to pitch

$$C_D(\theta) = A(v)\theta^2 + B(v)\theta + C(v) \quad (13)$$

Coefficient A

$$A(v) = A_1v^2 + A_2v + A_3 \quad (14)$$

where A_1 is 8.397, A_2 is −10.104, A_3 is 7.130.

Coefficient B

$$B(v) = B_1v + B_2 \quad (15)$$

where B_1 is 6.050, B_2 is −3.304.

Coefficient C

$$C(v) = C_1v^{C_2} \quad (16)$$

where C_1 is 1.068, C_2 is 1.700, C_2 is 1.700.

The specific constants obtained from Eqs. (13)–(16) for this test model are presented as above.

Table I provides a summary of the physical properties used in Eqs. (7)–(12). These properties were obtained directly from the 3D CAD model of the AUV. The hydrodynamic coefficients presented in literature are based on the model length and in non-dimensionalized form. The properties shown in Table I were used to convert the non-dimensionalized hydrodynamic coefficients derived from literature to obtain dimensionalized coefficients applicable to the modified SUBOFF model used in this research.

TABLE I. SUMMARY OF MODEL PROPERTIES

Attribute	Value
l_{hull}	1.15 m
ρ	1000 kg/m^3
m	2.5 kg
$\overline{V_h}$	0.005655 m^3
A_f	0.007854 m^2

Table II presents a summary of the hydrodynamic coefficents applicable to the DARPA SUBOFF model

used in this research. Coefficent values were obtained both through literature and the application of Strip Theory. Values that were obtained through experimental research in the literature were prioritised over calculated values due to the higher associated confidence levels. The exceptions are cases where the experimental values were not available in literature. The bold values were the ones selected to be carried into the digital model. Theoretical values of $X_{\dot{u}}$ were used over the data obtained by [18] due the higher values being a more conservative estimate. Additionally, the model used in [18] was not based off the SUBOFF project but was included in the table as a point of comparison as the two models were similar in size.

TABLE II. SUMMARY OF HYDRODYNAMIC COEFFICIENTS

Hydrodynamic Coefficent	Strip Theory [8, 20]	Exp. Results from Ref. [17]	Exp. Results from Ref. [16]	Exp. Results from Ref. [18]
$X_{\dot{u}}$	**1.00**			0.238
$Y_{\dot{v}}$	−5.655		**−12.31**	−15.37
$X_{u\|u\|}$	−1.31	**−1.49**		−2.126
$Y_{v\|v\|}$	0.899	**47.4**		20.57
$Z_{w\|w\|}$	0.899	**−55.7**		20.57
$M_{q\|q\|}$	**−2.426**			
$N_{r\|r\|}$	**−2.426**			

III. THEORETICAL MODEL CONSTRUCTION

A plant model was developed to study the dynamics of the AUV and to develop a robust controller to achieve the desired motion. The model allowed for real-time tuning and feedback from onboard sensors.

A. Open Loop Model

An open loop model was necessary to determine the steady-state characteristics of the model before control was implemented. This aided in establishing a theoretical baseline for system performance and responsiveness. Eqs. (1)–(6) were implemented in SIMULINK as a plant model with seven inputs representing the flow rates to each actuator jet (measured in m^3/s) and nine outputs representing angular velocities, angular rotations, and translational velocities as illustrated in Fig. 2.

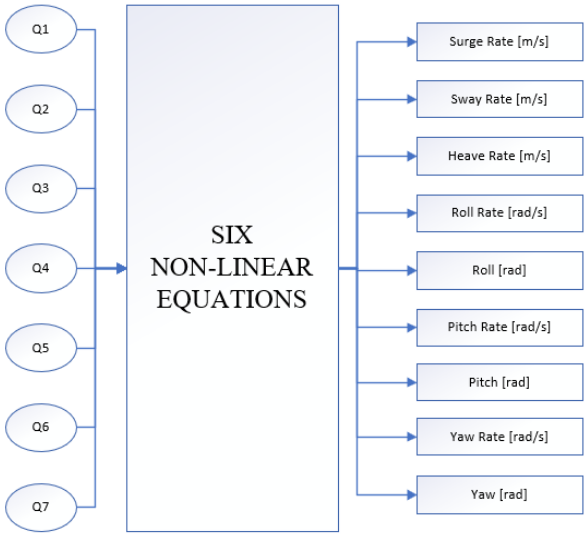

Fig. 2. Representation of analytical simulink model.

B. Conditional Switching Logic

The open loop characteristics were obtained by applying the maximum rated flow for the actuator pump (0.03 *L/s*) for the duration of the simulation according to the logic in Table III until a steady-state value was reached. These steady-state values represent the theoretical maximum values that the model can produce. During operation of the AUV, not all actuated jets were fired simultaneously, furthermore, the coupled nature of the jets necessitated a means of switching only the jets required for the specific motion. This conditional switching of jets was done by grouping jets together and assigning a value between 0–1 to these groups. This value represents a percentage of the maximum flow rate supplied by each pump, which corresponds directly to the operating speed (RPM) of a pump. Each group contained an independent PID controller to ensure the required flow rate was met, which resulted in a form of cascading PID control implemented in SIMULINK, as shown in Fig. 3.

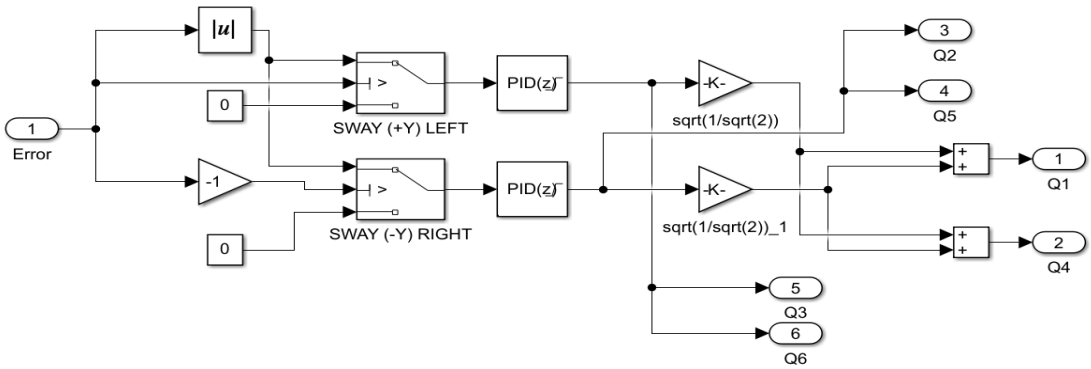

Fig. 3. Switching logic implementation.

TABLE III. CONDITIONAL SWITCHING LOGIC TABLE

	J1	*J2*	*J3*	*J4*	*J5*	*J6*	*J7*
+X	0	0	0	0	0	0	1
−X	0	0	0	0	0	0	0
+Y	0.841	0	1	0.841	0	1	0
−Y	0.841	1	0	0.841	1	0	0
+Z	1	0	0	1	0	0	0
−Z	0	1	1	0	1	1	0
+K	0	0	0	0	0	0	0
−K	0	0	0	0	0	0	0
+M	0	0.841	0.841	1	0	0	0
−M	1	0	0	0	0.841	0.841	0
+N	0.841	0	1	0.841	1	0	0
−N	0.841	1	0	0.841	0	1	0

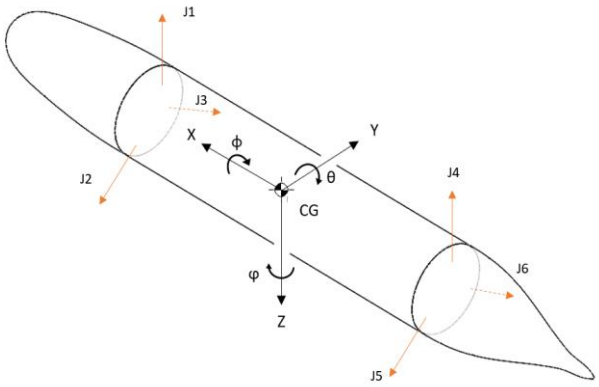

Fig. 4. Jet thruster orientation.

Table III contains the ratios required for any object containing 3 separate actuators spaced 120° apart. These ratios allow for independent axis motions from a coupled system. Fig. 4 provides a graphical description of the actuator orientations corresponding to Table III, where J1–J7 are the seven actuator jets. The cross section is viewed from the front of the model, where the +X axis is orientated out of the page and –X is into the page.

The conditional logic implementation in was fed into a filtered discretized PID algorithm [21], shown in Eq. (17), to obtain the required flow rate. This flow rate was then scaled according to the logic table to obtain the correct flow rate ratios for the actuators.

$$U(z) = K_p \left(\begin{matrix} 1 + K_i \cdot T_s \dfrac{1}{z-1} \\ +K_D \cdot \dfrac{N}{1 + N \cdot T_s \dfrac{1}{z-1}} \end{matrix} \right) E(z) \qquad (17)$$

C. Closed Loop Model

A closed-loop model was developed for the purpose of determining the controller gains, thereby reducing the number of experimental cycles required to refine the gains. The closed-loop model, shown in Fig. 5, was constructed with five functional blocks. Block A represents the open loop model from Fig. 2. The controller, shown in Block B, was connected to the input of Block A which contains the PID controllers and conditional switching logic from . Block C is the Inertial Measurement Unit (IMU), which records the angular accelerations and positions being fed to the comparator. Block D represents the sonars used for distance measurements from the pipe wall. Block E is a 3D visualisation block that creates a virtual model driven by outputs from the non-linear model to make a real-time representation of the AUV's orientation. The closed-loop response was obtained by simultaneously applying a set of commands from Table IV and recording the output from the data scopes.

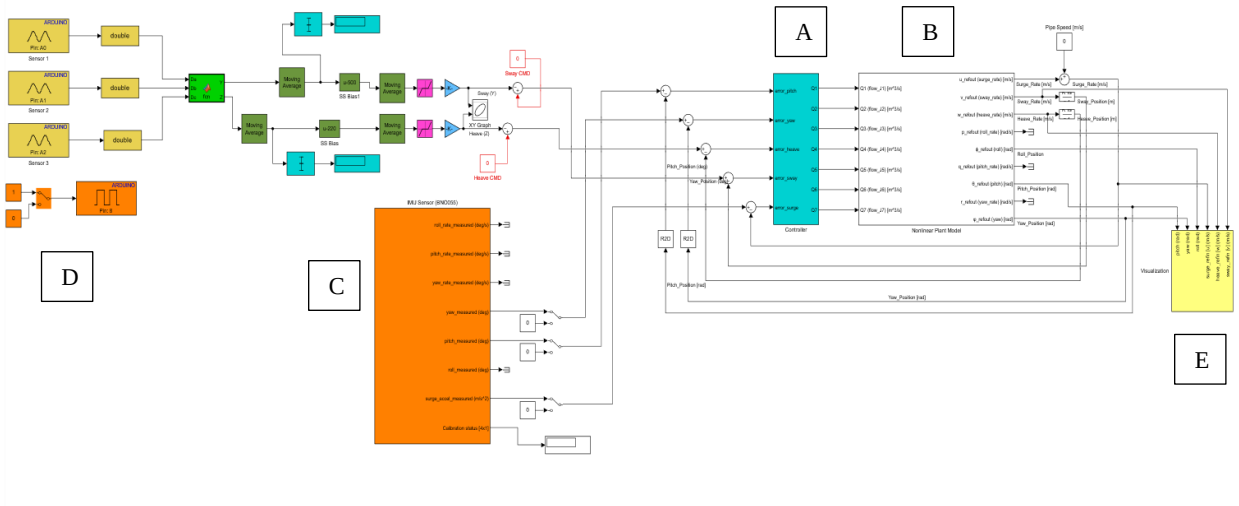

Fig. 5. Simulation implementation of the closed loop non-linear model.

TABLE IV. CLOSED LOOP COMMAND SUMMARY

Command Name	Config. 1	Config. 2
Surge Rate [m/s]	0	0
Sway Position [m]	0.1	−0.1
Heave Position [m]	−0.1	0.1
Yaw Position [°]	5	−5
Pitch Position [°]	10	−10

A Hardware-in-the-Loop (HIL) simulation was conducted. The closed-loop model was run in real time with the BNO055 IMU sensor being physically manipulated to provide a command input to the controller. The goal was to tune the controller such that the output from the dynamics model, and consequently the virtual 3D model, matched the orientation and tilt of the IMU. The virtualisation block displayed the output, and the controller gains were iteratively adjusted until the dynamics model output and IMU input matched. These tuned controller gains were then implemented in the AUV prototype for further experimentation and testing.

IV. TRIANGULATION OF PIPE WALL DISTANCES

Triangulation of sonar distance measurements was employed to estimate the AUV's position relative to the centerline of a pipe. This was achieved through the use of Euclidean geometry and vector algebra, as documented in Eqs. (18)–(25). Fig. 6 provides a graphical representation of the triangulation algorithm.

For accurate positioning, a minimum of three sonars were required. If spaced 120° apart, heave and sway could be estimated. Additionally, by having two sets of sonar arrays located fore and aft of the AUV, rotational motions can be estimated.

Note that rotational measurements were not incorpated into the triangulation algorithm, as an IMU sensor was implemented instead. During preliminary testing, the IMU was identified as a more reliable and direct way of measuring rotations.

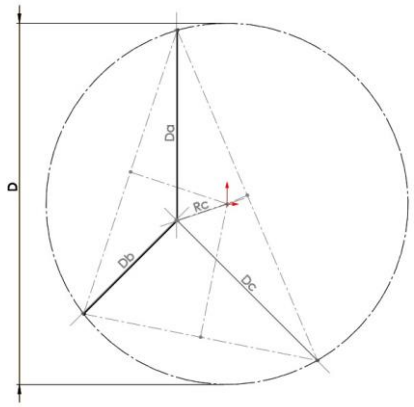

Fig. 6. Triangulation algorithm illustration.

The triangulation algorithm was implemented as a MATLAB function to efficiently utilise the built-in solving functionality to obtain a solution to Eq. (20). This function was imported into SIMULINK as a MATLAB function block. Due to the inherent nature of sonar measurements, a sliding average was applied to smooth out the signal between successive range finding to minimise the overshoot experienced by the model. It was found that a sliding average window of 15 s provided good results. The output from the function in the form of Heave and Sway was then fed back into the closed loop model to drive the heave and sway signals.

Based on Fig. 6, the required parameters for the algorithm were:

$$R = 0.5D$$
$$\theta = 45°$$
$$\overrightarrow{D_a} = \langle 0 \quad D_a \quad 0 \rangle$$
$$\overrightarrow{D_b} = \langle -D_b \cos\theta \quad -D_b \sin\theta \quad 0 \rangle$$
$$\overrightarrow{D_c} = \langle D_c \cos\theta \quad -D_c \sin\theta \quad 0 \rangle$$

The algorithm was executed through the following steps:

1) Calculate two sides of a triangle bound by a pipe wall by subtracting two distance vectors:

$$\overrightarrow{r_{AB}} = \overrightarrow{D_b} - \overrightarrow{D_a} \tag{18}$$

$$\overrightarrow{r_{AC}} = \overrightarrow{D_c} - \overrightarrow{D_a} \tag{19}$$

2) Find the midpoint of each length and take the cross product with an axis out of the page $\vec{z} = \langle 0,0,1 \rangle$ to obtain the centre line of the pipe.

3) Calculate the unit vector of each of the lines that intersect the centre:

$$\widehat{R_1} = \frac{\boldsymbol{r_{AB_{MID}}} \times \boldsymbol{z}}{\left\| \boldsymbol{r_{AB_{MID}}} \times \boldsymbol{z} \right\|} = \langle R_{1x} \quad R_{1y} \quad 0 \rangle \tag{20}$$

$$\widehat{R_2} = \frac{\boldsymbol{r_{AC_{MID}}} \times \boldsymbol{z}}{\left\| \boldsymbol{r_{AC_{MID}}} \times \boldsymbol{z} \right\|} = \langle R_{2x} \quad R_{2y} \quad 0 \rangle \tag{21}$$

4) Multiply each unit vector by an arbitrary length L_1 and L_2 to obtain a vector representation.

$$\overrightarrow{R_1} = L_1 * \widehat{R_1} \tag{22}$$

$$\overrightarrow{R_2} = L_2 * \widehat{R_2} \tag{23}$$

5) Sum vectors from the RHS to the centre and equate to the sum of vectors from the LHS to the centre and solve:

$$\overrightarrow{D_a} + \overrightarrow{r_{AB_{MID}}} + \overrightarrow{R_1} = \overrightarrow{D_a} + \overrightarrow{r_{AC_{MID}}} + \overrightarrow{R_2} \tag{24}$$

6) The position vector Rc can be found by equating to the sum of vectors around a loop and solving:

$$\overrightarrow{Rc} = \overrightarrow{D_a} + \overrightarrow{r_{AB_{MID}}} + \overrightarrow{R_1} \tag{25}$$

where position vector Rc represents the offset distanceof the AUV to the centre of the pipe.

V. Experimental Simulink Model

Once controller gains were suitably tuned using the model shown in Fig. 5, the tuned controller was transferred to an experimental SIMULINK model shown in Fig. 7. The non-linear plant model that was developed for tuning the controller, was not necessary for experimental testing and is omitted from the model in Fig. 7. Where Block A is the controller while Block B represents the flow rate to PWM signal conversion, which used a simple gain to complete the conversion. This gain was found by measuring the time taken to fill a known volume of water at varying PWM values.

Block C is comprised of the seven pump actuators driven by L293D drivers, which receive a PWM signal to drive the pumps.

The IMU sensor, shown in block D, was used to determine the AUV's orientation in the water and provide the result to the controller. Block E represents the control block where the target points are set. A reset switch was applied to the IMU with a trigger set to a rising edge. This trigger meant that the IMU would reset to zero at the start of the experiment to avoid past readings from influencing the test when it was conducted.

Block F represents the sonars and the triangulation algorithm that measures heave and sway. Block G was copied from the non-linear model and provided a visualisation of the AUV during the testing.

The roll axis was removed from the model as it was not actively controlled. The AUV relied on the metacentric relationship between the centre of gravity and buoyancy to maintain its upright position.

The experimental model was then connected to an Arduino Due through the built-in Arduino/SIMULINK library, allowing real-time communication with the Arduino microcontroller, together with the attached IMU sensor, pumps, drivers, and sonar sensors. This communication allowed real-time data capture of the pitch, yaw, heave, and sway.

The experiment was conducted in two parts. Part one investigated the sonar algorithm's heave and sway outputs around the pipe's centerline. The constant error bias and error range were then inferred from the data, and calibration was performed.

Part two investigated the pitch and yaw outputs of the IMU by commanding the AUV to pitch 5°, yaw at 5° and finally performing a combined 5° pitch + 5° yaw manoeuvre and recording the output from the IMU. The errors, bias and angular rates were then inferred from the results.

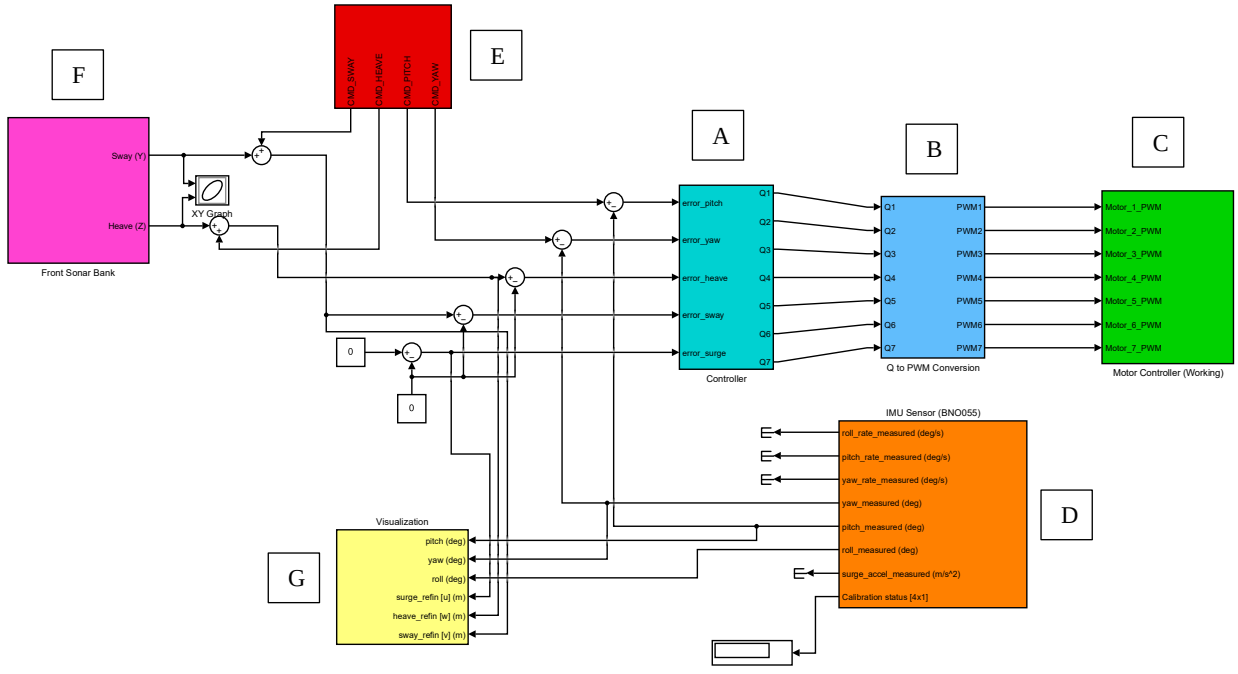

Fig. 7. Experimental implementation of the closed loop non-linear model.

VI. Results

This section presents open loop actuation response tests, the closed loop controller tests, the controller tuning parameters and the experimental results, which validate the theoretical plant model and controller design.

A. Open Loop Response

The open-loop surge command yielded a steady-state response in the velocity after 15 s corresponding to a maximum steady-state surge velocity of 0.2 m/s with an average maximum acceleration of 0.0133 m/s^2.

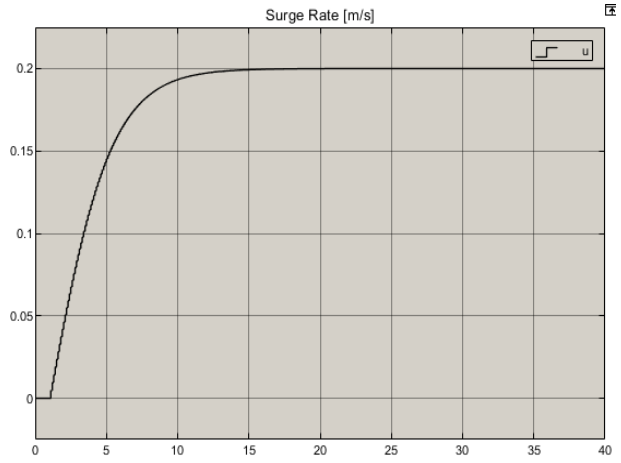

Fig. 8. Open loop surge response.

The open-loop pitch command yielded a steady-state response in the velocity after 5 s with a steady-state pitch velocity of 6.25°/s and a maximum acceleration of 1.25°/s^2.

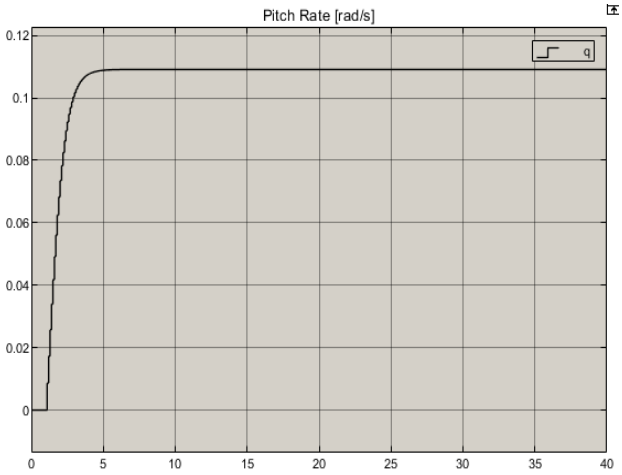

Fig. 9. Open loop pitch response.

Similar tests were conducted for the remaining axes of motion over a 40 s interval. The open loop responses are summarised in Table V.

TABLE V. SUMMARIZED OPEN LOOP RESPONSE

Axis of Motion	Max Velocity	Max Accel.
Surge	0.2 m/s	0.013 m/s2
Sway	0.0375 m/s	0.00125 m/s2
Heave	0.0406 m/s	0.00162 m/s2
Pitch	6.25 °/s	1.25 °/s2
Yaw	5.26 °/s	1.05 °/s2
Roll	N/A	N/A

The values show the theoretical maximum velocities and accelerations that the AUV can achieve at 100% output of the jet pumps with drag and inertia causing the system to reach steady-state. The nonsymmetry of the three jet design resulted in noticeable differences in speeds between antagonistic motions.

B. Closed Loop Response

The closed-loop controller slows the AUV's performance down but was a necessary trade-off for the ability to drive the system to target setpoints. The goal of the closed loop tests was to determine the impact of the tuned controller gains on the overall performance of the AUV, compared to the open-loop tests.

The closed-loop responses were obtained from two separate command strings, with the second being the inverse of the first. The controller was tuned iteratively in sequence, with an additional axis of motion being added to the tuning procedure every iteration, until all controlled axes were tuned.

The PID gains presented in Table VI achieved a good balance between robustness and responsiveness and the ability to handle a command string with six commands simultaneously:

TABLE VI. CLOSED-LOOP CONTROLLER GAINS

Axis of Motion	K_i	K_p	K_d	N
Surge	0.001	0.1	5	5
Sway	0.00045	0	20	5
Heave	0.001	0	10	10
Pitch	0.0005	0	0.5	5
Yaw	0.0002	0	1	10

The closed-loop system responses are recorded in Figs. 10 and 11 for each set of commands sent to the controller.

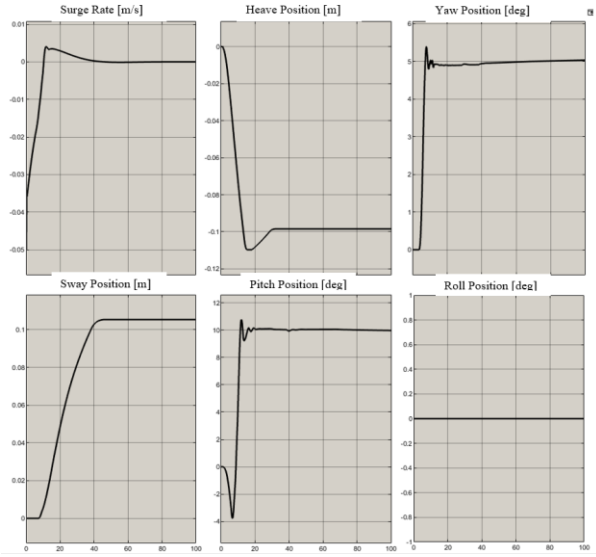

Fig. 10. Closed-loop system response for command set 1.

During tests the surge rate target was set to zero while a constant opposing flow of –0.05 m/s was applied. The controller was able to drive the model to a steady state around the desired operating point in approximately 40 seconds.

The summarized closed-loop performance for independent motion is shown in Table VII and does not include the model's performance when more than one command is given.

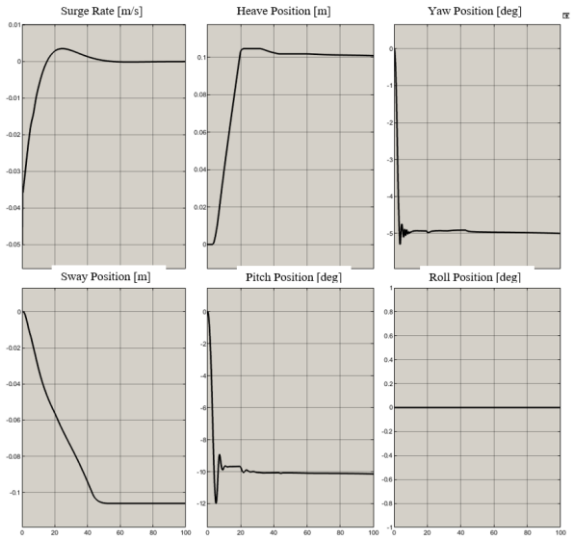

Fig. 11. Closed-loop system response for command set 2.

TABLE VII. SUMMARIZED CLOSED-LOOP RESPONSE FOR INDEPENDENT CONTROL

Axis of Motion	Max Velocity	Max Accel.
Surge	0.055 m/s	0.00275 m/s^2
Sway	0.008 m/s	0.0016 m/s2
Heave	0.012 m/s	0.0012 m/s2
Pitch	4.0 °/s	0.8 °/s2
Yaw	1.15 °/s	0.383 °/s2
Roll	N/A	N/A

Inferences from Figs. 10 and 11 were made to determine the translation and rotational speeds when the controller was given a complete set of commands simultaneously. This method mimicked a more practical application of the controller. Table VIII summarizes the closed loop response.

TABLE VIII. OVERALL CLOSED LOOP RESPONSE

Axis of Motion	SET 1	SET 2
Surge (m/s)	0.0055	0.0055
Sway (m/s)	0.00367	−0.0244
Heave (m/s)	−0.00286	0.00250
Pitch (°/s)	0.5	−0.5
Yaw (°/s)	0.25	−0.5
Roll (°/s)	N/A	N/A

The open loop responses from Table V were compared with the closed loop responses from Tables VII and VIII. Pitch and Surge steady-state maximum speeds saw a 36% and 72.5% decrease respectively with an increased latency of 10 s and 25 s, respectively. The closed-loop steady-state performance for independent motions was worse than the open-loop performance, as expected. If multiple commands were given simultaneously then the AUV's performance dropped. Closed-loop responsiveness increased as the controller errors become smaller, due to a reduced demand on the controller. The response times of the system can be improved with further research and development. For the purpose of the project at hand the performance was deemed acceptable, considering the tradeoff between system size, cost and performance. The ability to drive the AUV to a target position and maintain a steady pose within 40 seconds was deemed acceptable for pipe inspection purposes.

C. Experimental Results

1) Triangulation algorithm to estimate heave and sway

This experiment investigated the effectiveness of the sonar triangulation algorithm. The objective of the experiment was to determine the accuracy of Y–Z measurements of the AUV relative to the pipe wall and was achieved through two dry tests shown in Fig. 12. Uncalibrated output from the triangulation algorithm was recorded as a baseline.

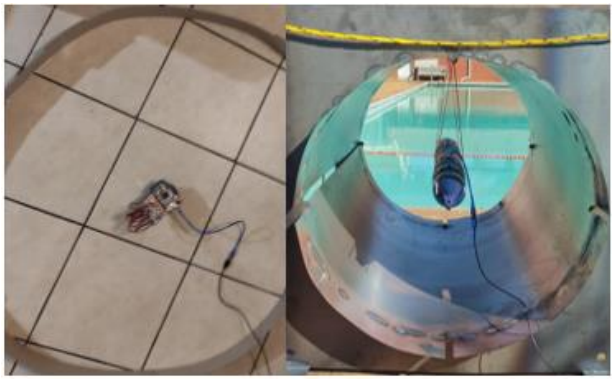

Fig. 12. Dry test set-up of sensor test.

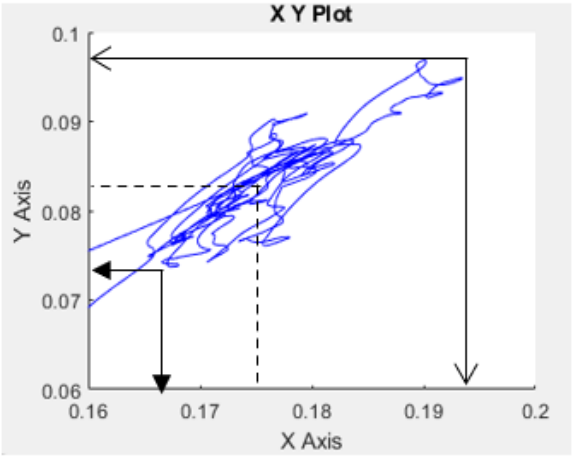

Fig. 13. Uncalibrated sensor output.

After a simulation time of 450 s with a sample time of 0.1 s, the mean bias in the X and Y frame was approximately $\langle 0.175,\ \ 0.084\rangle$ m from the centre of the pipe. The X axis error was in the range of $-0.009 \leq X_{error} \leq 0.02$ m, while the Y axis error was in the range of $-0.01 \leq Y_{error} \leq 0.014$ m, measured from the mean position, shown in Fig. 13. This offset was more apparent when viewed with a virtual model shown in Fig. 14. The transparent circular region represents the pipe area, and the smaller circle represents the AUV model viewed from the rear.

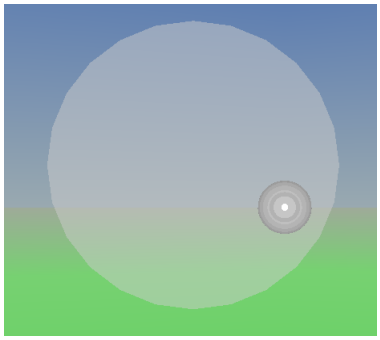

Fig. 14. 2D Uncalibrated visualization.

For a simulation time of 205 s with a sample rate of 0.1 seconds, the mean bias of the calibrated sensor in the X and Y frame was approximately $\langle -0.005, \ 0.004 \rangle$ m from the centre of the pipe. The X axis error range was $-0.007 \leq X_{error} \leq 0.004$ m, while the Y axis error range was $-0.004 \leq Y_{error} \leq 0.006$ m, measured from the mean position, as shown in Fig. 15.

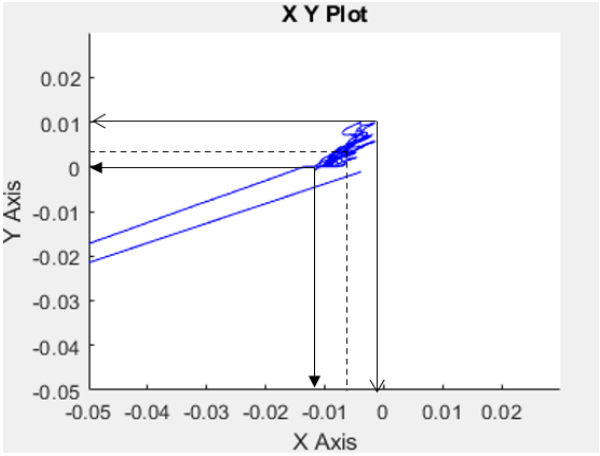

Fig. 15. Calibrated sensor output.

The calibrated result was superimposed on the uncalibrated result obtained and shown in Fig. 16. The summarized results of the algorithm performance were recorded in Table IX, which showed the bias and steady-state errors after calibration. A significant improvement in the approximation of the AUV's position was noted after the calibration procedure was complete, as illustrated in Fig. 16.

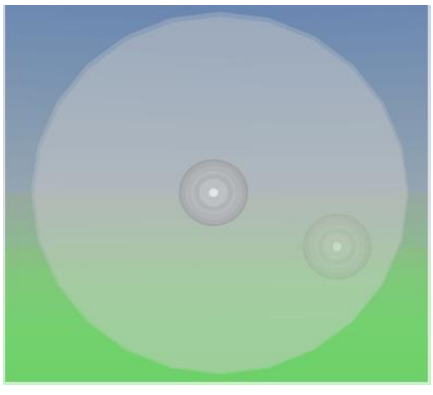

Fig. 16. 2D calibrated visualization.

TABLE IX. SUMMARIZED TRIANGULATION ALGORITHM RESULTS

Axis of Motion	Error (m)
Heave (Y) Constant-Bias Error	0.004
Sway (X) Constant-Bias Error	−0.005
Average Heave (Y) Steady State Error	±0.0033
Average Sway (X) Steady State Error	±0.001
Max/Min Heave (Y) Error	0.004/−0.007
Max/Min Sway (X) Error	0.006/−0.004

2) Control response to pitch and yaw

This experiment investigated the accuracy of the HIL testing compared to actual performance of the AUV platform in a pool. The test was conducted by commanding pitch to 5° with zero yaw, followed by yaw to 5° with zero pitch and finally, a combined 5° command to both pitch and yaw. The test results were obtained in real-time from data logging through SIMULINK.

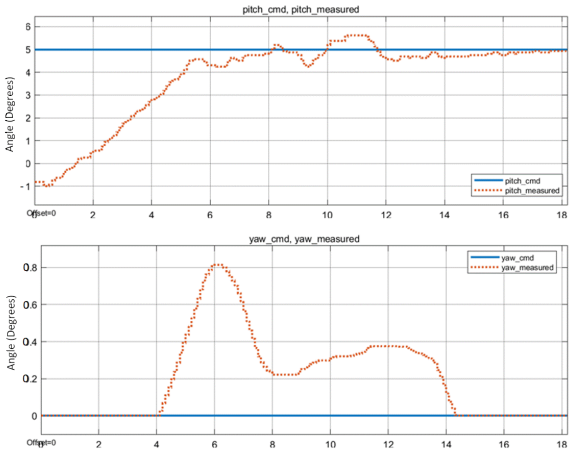

Fig. 17. Response from 5° pitch command.

The system response when given a 5-degree pitch command is shown in Fig. 17. The system experienced a maximum overshoot of 5.6° above the target and reached the 5-degree target at 8 s. The irregular signal was due to signal noise and turbulence in the water. Between 2 to 4 s, the pitch rate is constant, with a maximum pitch rate of 1.25 °/s.

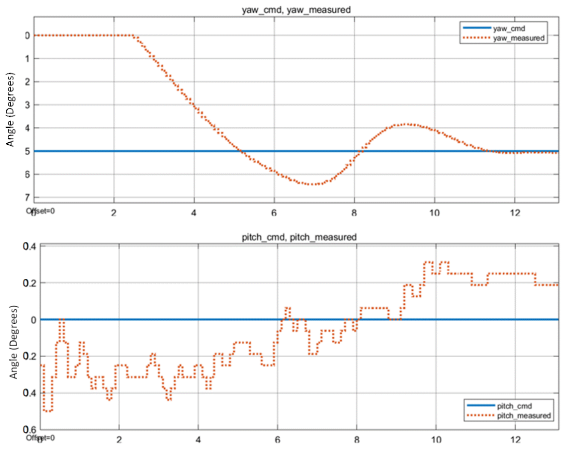

Fig. 18. Response from 5° yaw command.

The yaw command shown in Fig. 18 was significantly smoother than the pitch due to the aggressive filtering implemented to integrate the yaw rate. The maximum overshoot was 30% of the command with an error of −1.5° under the target. The pitch command averaged to approximately zero but showed the turbulence of the water more clearly. The maximum average yaw rate of 1.78°/s was observed between 2.2 s and 5 s, crossing the 5-degree mark.

Pitch and Yaw test data are respectively shown in Figs. 17 and 18, which presented the non-zero responses in yaw and pitch respectively when given only a single command. The non-zero yaw during pitching of the AUV is due to the inherent coupled nature of the system dynamics and orientation of the jet actuators. The 120° spacing of the jets resulted in shared force components that were not entirely eliminated by the controller. The same reasoning applies to the presence of a non-zero pitch during a yawing motion of the AUV. The non-zero components are relatively small and while they may be reduced by further tuning of the second derivatives the results were deemed acceptable.

The control of two commands simultaneously required more control effort than a single command. Fig. 19 shows an image taken from the side of the pool during the combined pitch and yaw command to demonstrate the response of the AUV with reference to the line of the shadow of the pool edge.

Fig. 20 showed that the maximum pitch overshoot was 30%, with an error of 1.5°, and the constant bias error was approximately 1°. The overshoot for yaw was less than the pitch at 16%. With a combined command, the average pitch and yaw rates were 1.5°/s and 1.25°/s, respectively.

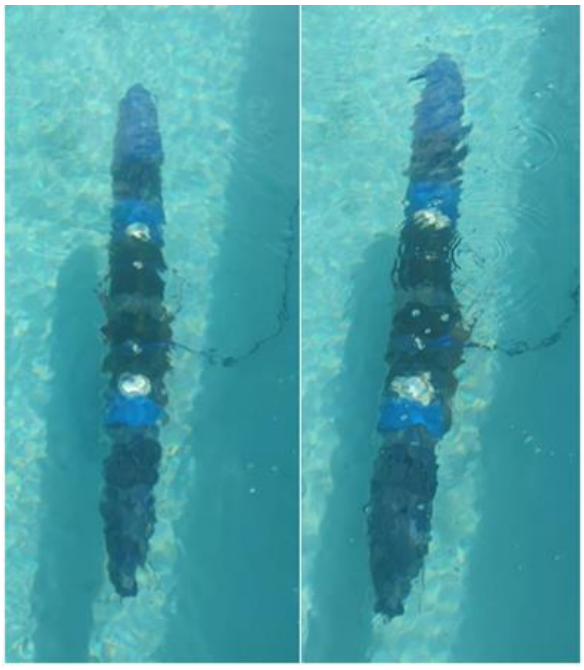

Fig. 19. Yawing of the AUV.

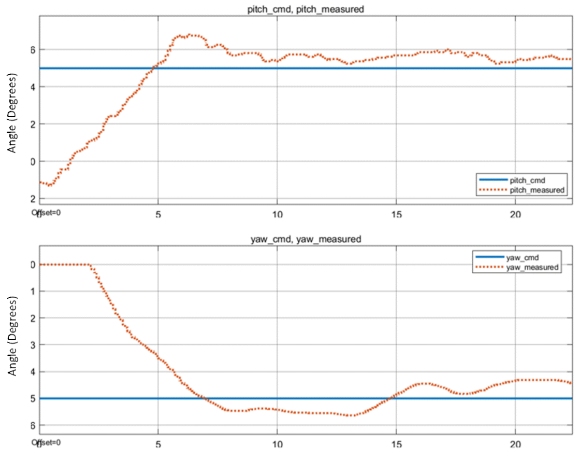

Fig. 20. Response from combined 5° pitch and yaw.

The system was approximately 8% faster in settling on heave commands than sway. The difference was due to the jet configuration, with two jets positioned near the bottom and a single jet at the top of the AUV. The chosen configuration aided positive heave and pitch motions. Consequently, negative commands of heave and pitch were expected to be slower than positive ones.

D. Closed Loop Response

Negative commands produced a noticeable overshoot in pitch and heave graphs. This was attributed to unbalanced forces, with an underpowered reaction force for positive pitch and heave actions. The observation is supported by the pitch and heave speeds being noticeably higher than yaw and sway.

Maximum sway accelerations were higher than expected, when compared to the open loop response. This was attributed to human error in accurately measuring the accelerations.

Pitch showed a significantly faster response time than yaw, with as much as twice the acceleration. The cause was the horizontal component of a single jet thrust vector contributing to yaw motions which contrasted with the pitch having two jet vectors contributing to its movement. This can be improved by revisiting the design to include an additional jet actuator to balance the forces on both sides. This would have the added benefit of decoupling the forces to an extent and simplifying both the logic switching and computational load on the controller.

E. Experimental Results

Initial start-up of the testing model identified discontinuities in the sonar graphs, which showed strong spikes that went out of bounds but soon stabilized. These were not able to be removed entirely but were mitigated through aggressive filtering which consequently made the sonar system sluggish when detecting short disturbances. The addition of the IMU sensor meant that two redundant measuring systems were used to infer readings.

From this, a significant finding was in the use of the triangulation algorithm which could theoretically allow for the sonars to work without accounting for the density of

water as only the relative distance between two sonar readings would be required.

The IMU responded well during experimental testing and was able to detect minor disturbances caused by turbulence and filter out much of the high frequency inputs, however drift errors were discovered when double integrating the accelerometer readings to obtain linear estimates, hence, the sonar readings were prioritized in these cases. Future work includes implementing direct linear measurements, possibly through sonar doppler estimates to reduce reliance on drift-prone measurements.

The yaw command showed a delay over the pitch command signifying a weaker actuation force than pitch commands. The layout of the jets supported the observation. Nearly all available jet force was used to drive pitch and heave, while only half of the force was utilized by yaw and sway motions. This layout meant it would take roughly twice as long to reach the setpoint for yaw. The arrangement of the jets, adding more jets and increasing the pump size are possible solutions toward improving settling times and creating a more balanced system.

One significant source of error identified during experimentation was the turbulence in the pool which affected the consistency of results. Despite the turbulence, the AUV handled the disturbance and reached its target setpoints, validating the controller design and plant modelling.

F. Theoretical and Experimental Model Comparison

Open loop performance established the AUV's theoretical maximums regarding speed and accelerations. Closed Loop performance suffered due to the amount of switching and the robust design of the controller, sacrificing response time for stability. In terms of proportions, Open Loop Performance from the digital model and ratios obtained from the Closed Loop performance from testing were compared:

$$\frac{\text{Heave}_{\text{OL}}}{\text{Sway}_{\text{OL}}} = \frac{0.0406}{0.0375} = 1.08 \qquad \frac{\text{Heave}_{\text{CL}}}{\text{Sway}_{\text{CL}}} = \frac{0.0029}{0.0037} = 0.78$$

$$\frac{\text{Pitch}_{\text{OL}}}{\text{Yaw}_{\text{OL}}} = \frac{6.25}{5.26} = 1.19 \qquad \frac{\text{Pitch}_{\text{CL}}}{\text{Yaw}_{\text{CL}}} = \frac{1.5}{1.25} = 1.2$$

The values showed that there was a proportional relationship between the digital model and the experimental model. The ratio of translational motions between the digital and experimental models differed by 30%, partly due to the inaccuracies found during testing of the sonars. The digital model was also limited in that it did not consider turbulence, which was present in the pool tests. The rotational motions showed better accuracy, with a difference of 0.83% between the digital model and experiments. The correlations between the axes of motion suggest some value in using the digital model to estimate the experimental performance with the application of a scaling factor. Pitch and yaw showed the best accuracy, while heave and sway showed a higher degree of uncertainty attributed to the anchoring of the AUV during pool tests, which limited the natural heave and sway of the AUV.

Although no comparable architectures for DARPA SUBOFF AUV models were found in literature, specifically in the usage context of in-pipe inspections, the control algorithm performance can be compared with similar in-pipe robots such as Kazeminasab *et al.* [22] and Painumgal *et al.* [23] to determine comparable performance, Tables X and XI show these tabulated performance metrics.

TABLE X. PITCH AND YAW COMPARISON WITH EXISTING LITERATURE

	PTICH			YAW		
Criterion	**REF**	**[22]**	**[23]**	**REF**	**[22]**	**[23]**
Target (°)	5	0	0	−5	0	0
Settle Time (s)	12	2.3	5.4	12	1.5	23
Overshoot (°)	0.6	2.6	−5	−1.5	1.2	−3.3
Rise Time (s)	8	1	2.5	5.3	0.8	5.2
Initial Value (°)	−1	−10	13	0	5	−8
%OS	10	26.5	38.5	30	24	41

TABLE XI. SWAY (X) AND HEAVE (Y) COMPARISON WITH EXISTING LITERATURE

Criterion	REF	[23]	Criterion	REF	[23]
Target (mm)	0	0	Target (mm)	0	0
Constant Bias (mm)	−5	2.6	Constant Bias (mm)	4	−3.1
Average X error (mm)	6/−4	21.9/−16.8	Average Y error (mm)	4/−7	8.9/−15

The comparative study showed that the control algorithm presented in this paper shares similar performance with existing literature, with lower overshoots at the expense of slower rise and settle times. However, it should be noted that the physical geometry and mechanical actuation of these in-pipe robots differ significantly, which plays a role in the performance differences of the controllers.

VII. CONCLUSION

Failing pipelines have a significant economic impact. Proactive steps must be taken in conducting timely maintenance of pipes before failure occurs.

This study investigated a potential solution in developing a low-cost platform with the potential to be used as a pipe inspection AUV, which can operate in pipelines without impacting daily operations.

The study identified equations of motion and hydrodynamic coefficents for the AUV profile. The theoretical model agreed well with experimental results when a correction factor was applied; however, work still needs to be done to improve the accuracy of heave and sway measurements taken about the pipe wall. The study found that a 3-jet design, although simple, required a more complicated switching control system to obtain independent axis control and produced unbalanced results in certain manoeuvres with slower response times in sway and yaw compared to pitch and heave.

The results show that a theoretical model based on the standard equations of motion for a submarine can be effectively used to develop a controller without expensive experimental iterations, significantly lowering design time and cost. Future work includes investigating stateflow switching to improve response times.

NOMENCLATURE

Roman

A_j	Jet orifice area [m^2]
A_f	Test model frontal area [m^2]
B	Buoyant Force [N]
I_i	Inertia along direction *i* [kg.m^2]
L_j	Distance from CoG to jet [m]
l_{hull}	Length of test model [m]
m	Mass [kg]
$M_{q\|q\|}$	Added Mass M due to product q^2 [kg.m^2]
$N_{r\|r\|}$	Added Mass N due to product r^2 [kg.m^2]
p	Pitch rate [rad/s]
q	Yaw rate [rad/s]
Q_j	Jet flow rate [m^3/s]
r	Roll rate [rad/s]
T_s	Discretized time sample step [s]
u	Surge [m/s]
v	Sway [m/s]
$\overline{V_h}$	Hull volume [m^3]
W	Weight [N]
w	Heave [m/s]
$X_{\dot{u}}$	Added mass X due to velocity *u* [kg]
$X_{u\|u\|}$	Added mass X due to product u^2 [kg/m]
$Y_{\dot{v}}$	Added mass Y due to velocity *v* [kg]
$Y_{v\|v\|}$	Added mass Y due to product v^2 [kg/m]
$Z_{w\|w\|}$	Added mass Z due to product w^2 [kg/m]

Greek

α	Angle of Attack (Pitch) [°]
β	Angle of Attack (Yaw) [°]
ρ	Density of fluid [kg/m^3]
θ	Euler-Pitch [°]
φ	Euler-Yaw [°]
ϕ	Euler-Roll [°]

Abbreviations

AUV	Autonomous Underwater Vehicle
HIL	Hardware-In-Loop
PIG	Pipe Inspection Gauge
CFD	Computational Fluid Dynamics
IMU	Inertial Measurement Unit

CONFLICT OF INTEREST

The authors declare no conflict of interest.

AUTHOR CONTRIBUTIONS

Tazden Sewell conducted the research, performed the experiments and analyzed the data as part of a postgraduate research project. Jared Padayachee supervised the development of the electronic control system and Glen Campbell Snedden supervised the development of the CFD model. All authors wrote the paper and revised the manuscript. All authors approved the final version.

REFERENCES

[1] Here's how much water SA loses through water leaks. *Infrastructure News*. (6 March, 2017). [Online]. Available: https://infrastructurenews.co.za/2017/03/06/heres-how-much-water-sa-loses-through-water-leaks/

[2] B. Reed, "California oil spill pipeline had been left to rust paper-thin," *The Guardian*, Santa Barbara, 2015.

[3] P. Boughton. (21 February, 2013). EngineerLive. [Online]. Available: https://www.engineerlive.com/content/internal-and-external-inspection-submerged-pipelines

[4] M. Beller and C. E. S. Ponce, "Options for Internal inspection of difficult-to-check pipelines," *Pipeline & Gas Journal*, vol. 248, no. 6, 2021.

[5] iPEK International GmbH. (May 2023). Kanal-TV inspection. [Online]. Available: https://www.ipek.at/fileadmin/user_upload/broschueren/ipek_komplettbroschuere_de.pdf

[6] X5-HR Screw Type Crawler. (2022). *Easy-Sight*. [Online]. Available: https://www.pipedetect.com/products/x5-hr-sewer-robot-camera/

[7] Spot-The Agile Mobile Robot. (2023). *Boston Dynamics*. [Online]. Available: https://bostondynamics.com/products/spot/

[8] PIBOT. (2023). KNR Systems Inc. [Online]. Available: http://www.knrsys.com/portfolio/electric-based-robot-2/

[9] THESBOT-Dual. HiBot. (2022). [Online]. Available: https://www.hibot.co.jp/products/thes-dual/

[10] A. Nayak and S. K. Pradhan, "Design of a new in-pipe inspection robot," *Procedia Engineering*, vol. 97, pp. 2081–2091, 2014.

[11] K. Hayashi, T. Akagi, S. Dohta, W. Kobayashi, T. Shinohara, K. Kusunose, and M. Aliff, "Improvement of pipe holding mechanism and inchworm type flexible pipe inspection robot," *International Journal of Mechanical Engineering and Robotics Research*, vol. 9, no. 6, pp. 894–899, 2020.

[12] Y. Wu, A. Noel, D. D. Kim, K. Youcef-Toumi, and R. Ben-Mansour, "Design of a maneuverable swimming robot for in-pipe missions," in *Proc. International Conference on Intelligent Robots and Systems (IROS)*, Hamburg, 2015.

[13] F. Nickols, D. Ho, S. O. Harrold, R. T. Bradbeer, and L. Yeung, "An ultrasonically controlled robot submarine for pipe inspection," in *Proc. Fourth Annual Conference on Mechatronics and Machine Vision in Practice*, Australia, 1997.

[14] N. C. Groves, T. T. Huang, and M. S. Chang, G*eometric Characteristics of Darpa Suboff Models (DTRC Model nos. 5470 and 5471)*, David Taylor Research Center, Bethesda, MD, 1989.

[15] G. Hagen and M. Gertler, "Standard equations of motion for submarine simulation," Naval Ship Research and Development Center, 1967.
[16] Y. C. Pan, H. X. Zhang, and Q. D. Zhou, "Numerical prediction of submarine hydrodynamic coefficients using CFD simulation," *Journal of Hydrodynamics*, vol. 24, no. 6, pp. 840–847, 2012.
[17] K. Takahashi and P. K. Sahoo, "Numerical study on the hydrodynamic performance of the darpa suboff submarine for steady translation," in *Proc. International Conference on Ocean, Offshore & Arctic Engineering, Fort Lauderdale*, FL, 2020.
[18] P. Ridley, P. Corke, and J. Fontan, "Submarine dynamic modeling," Queensland University of Technology, Brisbane, 2015.
[19] F. H. Imlay, "The complete expressions for 'Added Mass' of a rigid body moving in an ideal fluid," Hydromechains Laboratory Research and Development Reprot, Department of the Navy, David Taylor Model Basin, 1961.
[20] T. Sia Chuan, "Modeling and simulation of the autonomous underwater vehicle, autolycus," Massachusetts Institute of Technology, Massachusetts, 1999.
[21] PID Controller. (2009). *MathWorks*. [Online]. Available: https://www.mathworks.com/help/simulink/slref/pidcontroller.html
[22] S. Kazeminasab, A. Akbari, R. Jafari, and M. K. Banks, "Design, *characterization, and control of a size adaptable in-pipe robot for water distribution systems*," in *Proc. 22nd IEEE International Conference on Industrial Technology (ICIT)*, Valencia, Spain, 2021.
[23] U. V. Painumgal, B. Thornton, T. Uray, and Y. Nose, "Positioning and control of an AUV inside a water pipeline for non-contact in-service inspection," in *Proc. 2013 OCEANS*, San Diego, 2013.
[24] D. Sachs, "Sensor fusion on android devices: A revolution in motion processing," *Google TechTalks-InvenSense*, 2010.